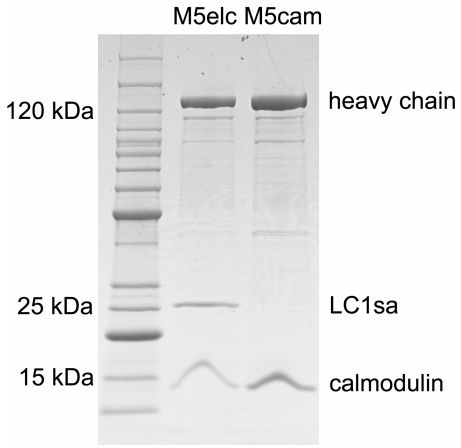

Figure S1. Samples of M5elc and M5cam run on a Tris-HCl Biorad 4-20 % gradient polyacrylamide gel (161-1123). The lane containing M5elc shows the presence of LC1sa, and the lane containing M5cam does not.

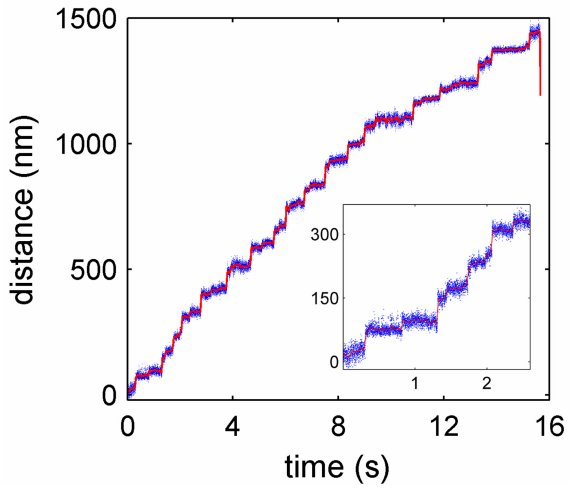

Figure S2. Example trace showing alternating 21 and 53 nm steps. Data were collected with M5elc, 3 μM ATP, 40 nm diameter gold particle label, and 3125 Hz frame rate. The data are overlaid with a 32 ms sliding average (*red*). The inset shows the first ~2.5 s of the trace.

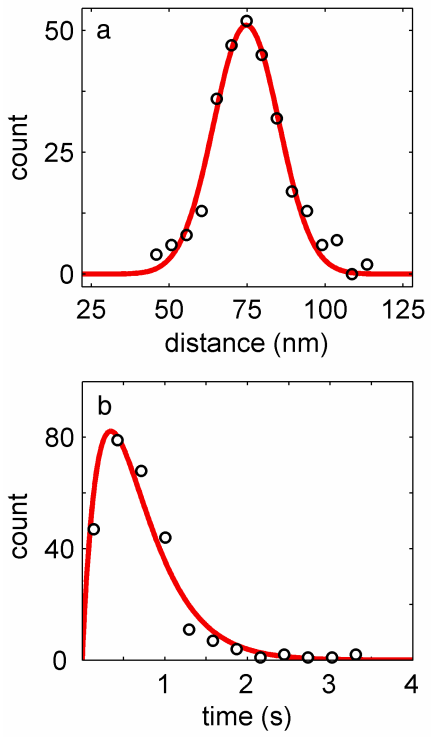

Figure S3. Displacement and dwell time distributions for M5elc. Traces were recorded at rates between 100 and 3125 Hz, with 40 and 60 nm diameter gold particles. (a) Step size histogram. The distribution was fit to a Gaussian; 288 steps, center = 74.7 ± 0.9 nm, standard deviation = 10.5 nm. (b) Dwell time histogram. Two sequential 37 nm steps, each with rate k, yield the observed 75 nm displacement; k = 2.9 ± 0.1 s^{-1}. The average dwell time was 0.70 s, corresponding to a maximum likelihood estimate (mle) for k of 2.8 s^{-1} (see Methods).

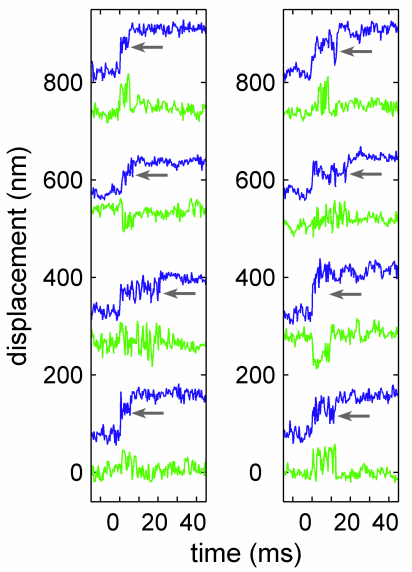

Figure S4. Sample M5elc 49 nm substeps recorded at 3125 Hz, using 40 nm gold particles. The displacement along the actin filament is shown in *blue*. The corresponding perpendicular displacement is shown immediately below in *green*. The end of the substep is indicated by a gray arrow. Note the increased variance in both directions during the intermediate. Transient lateral offsets were observed to both the left (positive) and right.

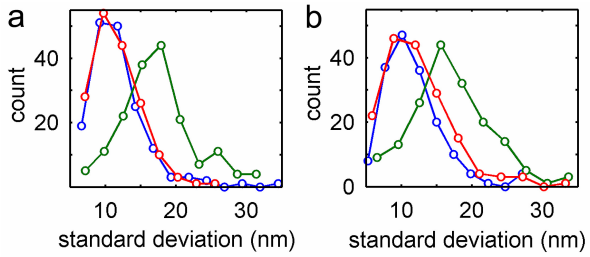

Figure S5. The bead explores a larger space during the substep than before or after. (*a*) Histograms showing the axial position standard deviation for 9.6 ms before (*blue*; ave. = 11.8 nm), during (*green*; ave. = 17.5 nm) and 9.6 ms after (*red*; ave. = 11.7 nm) the substep. (b) Histograms showing the lateral position standard deviation for 9.6 ms before (*blue*; ave. = 11.5 nm), during (*green*; ave. = 16.9 nm) and 9.6 ms after (*red*; ave. = 12.2 nm) the substep. All data were recorded at 3125 Hz using M5elc and 40 nm Au. N = 167. Only steps with intermediates lasting 1.6 ms or longer are included in this analysis.

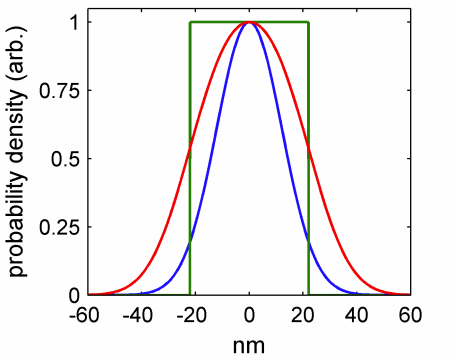

Figure S6. The convolution (*red*) of a 12 nm standard deviation Gaussian (*blue*) and a -22 to 22 nm uniform probability distribution (*green*). All the curves are scaled with a maximum of 1 arbitrary unit.

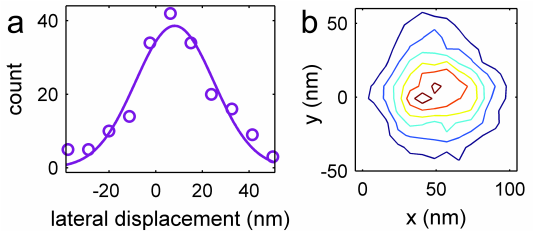

Figure S7. Lateral displacement during the intermediate. Data are calculated for M5elc labeled with 40 nm Au, and recorded at 3125 Hz. (*a*) Histogram of lateral displacements during the one-head bound intermediate, showing an average of 8.0 ± 1.2 nm (N = 192, s.d. = 16.3 nm). The large s.d. may result from molecules which walk at varying angles to the slide surface, or possibly from variation in the Au-myosin attachment. (*b*) Contour plot of the 2D distribution of data points compiled from the intermediates of 192 steps. The distribution is calculated relative to a starting position at (0, 0) corresponding to the average of the data points recorded in the 32 ms prior to the step. The distribution is fit to a double Gaussian with μ_x = 51 nm, μ_y = 4.0 nm, σ_x = 23.6 nm, σ_y = 22.3 nm. μ_x and μ_y reflect the average axial and lateral offsets during the one-head bound state. σ_x and σ_y are increased relative to the distribution in Figure 2b because they include the static variation in position.

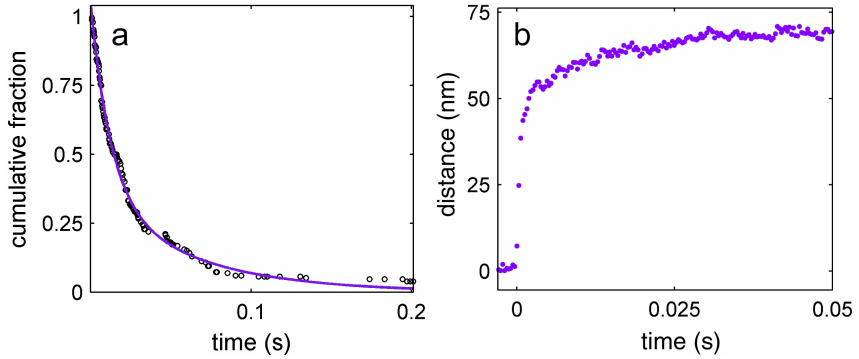

Figure S8. *(a)* The unhindered M5elc free head rebinding rate is 80 ± 13 s^{-1} in the presence of 100 mM BDM (n = 232). *(b)* 202 synchronized and averaged steps recorded for M5elc in the presence of 3 μM ATP, 100 mM BDM, 3125 Hz frame rate. The rise to ~50 nm is response-limited.

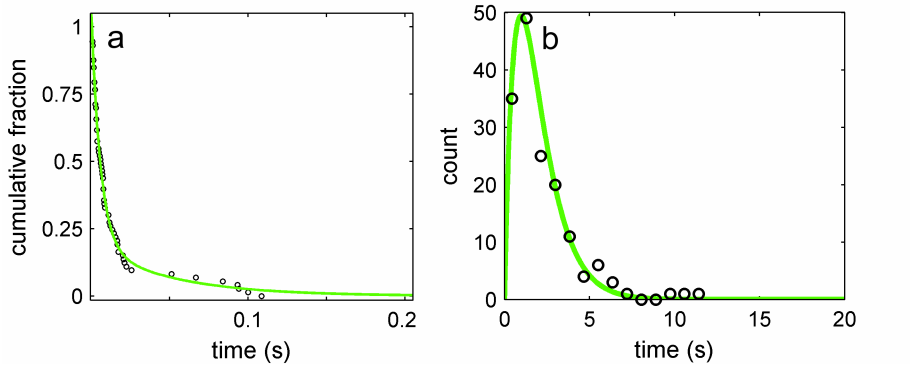

Figure S9. (*a*) The M5elc free head rebinding rate measured in the presence of 50 mM phosphate is 170 ± 40 s^{-1}, (n = 73). (*b*) However, the underlying ATP turnover rate *k* is slowed to 1.0 ± 0.1 s^{-1} (n = 157). The average dwell time is 2.2 s, corresponding to a mle for *k* of 0.9 s^{-1}.

SUPPLEMENTARY INFORMATION Dunn and Spudich, 2007

Simulation of one-head bound state

Using the coordinate system:

$$x = \cos(\theta)\sin(\varphi)$$
$$y = \sin(\theta)\sin(\varphi)$$
$$z = \cos(\varphi)$$

The surface area element of a sphere is $d\Omega = \sin(\varphi)\, d\theta\, d\varphi$. Integrate θ from 0 to 2π: $d\Omega = 2\pi \sin(\varphi)\, d\varphi$. Note that $dz = -\sin(\varphi)d\varphi$, so $d\Omega = -2\pi\, dz$. This shows that the density of points is constant along z, or any other axis.

The observed distribution of data points during the one-head bound intermediate is therefore the convolution of a step function and the roughly Gaussian noise inherent in the measurement. The series treatment of the convolution operation was used to numerically simulate the result:

$$(f * g)(m) = \sum_n f(n)g(m-n)$$

Here f is a Gaussian and g is a uniform distribution. The * symbol is the convolution operator. The resulting distribution is approximately Gaussian, with a width of 18 nm, in agreement the observed increase in standard deviation during the intermediate.

The above analysis assumes that the lever arm of the attached head is absolutely rigid. However, previous measurements suggest that the myosin V lever arm stiffness is about 0.25 pN nm^{-1} (ref. 1). Using the equipartition theorem, this indicates that the end of the bound lever arm should fluctuate with a standard deviation of about 4 nm. In this model, we therefore have *three* distributions to convolve: a 12 nm Gaussian, a 4 nm Gaussian, and a step function of some width. The convolution of the two Gaussians is another Gaussian with a standard deviation of $(12^2 + 4^2)^{½} = 12.65$ nm. Convolving a -20 to 20 nm uniform probability distribution with this widened Gaussian results in a pseudo-Gaussian curve with a standard deviation of 18 nm (thus matching the data). Thus, in the modified model the effective lever arm length is 20 instead of 22 nm.

We also briefly consider other possible models for the one-head bound intermediate. For instance, the particle could be imagined to rotate only in the *xy* plane, parallel to the slide surface. A similar calculation to that above indicates that a lever arm length of 17 nm would fit

the observed s.d. increase. However, it is difficult to envision a physically reasonable model for how the free head could be constrained to rotate in the *xy* plane. In contrast, the model with free rotation of the unbound head requires only a free swivel between the lever arm and coiled-coil domain. Dramatically softened lever arm stiffness, either throughout its length or in the converter region, could also in principle account for the observed s.d. increase. This scenario would correspond to a lever arm spring constant of 0.023 pN nm^{-1}, which is ~10-fold less than commonly accepted values for the myosin V lever arm[1]. In addition, in this model the one-head bound intermediate would bend backwards 43 nm under a 1 pN load, making processive stepping unlikely.

Half of the runs end in a 50 nm step with increased variance

We noted that about half of the last steps in processive runs shared similarities with this intermediate: a ~50 nm displacement and increased variance relative to the previous steps (Figure 1b is an example). In order to avoid selection bias, we examined all the last steps in runs that terminated in particle detachment (not the end of a data file). For 41 such last steps, the *average* displacement and dwell time was 62 nm (the average of 74 nm and 49 nm) and 0.49 s. The noise in these last steps had a higher standard deviation (15.4 nm) than that of the previous steps (12.0 nm). Thus, these results are consistent with the presence of two equal populations, one that matches the previous steps (74 nm displacement, 12 nm noise) and one similar to the intermediate (49 nm displacement, 18 nm noise).

Both the 49 nm substep and half of the last steps therefore correspond to a one-head bound state. Most of the processive runs we observe end when the unattached head is unable to rebind, leading to a prolonged one-head bound state.[2] If the attached head is labeled, the last observed displacement is a full 74 nm. However, if the detached head is labeled, the last observed displacement is 49 nm, corresponding to the one-head bound state. The duration of this state is determined by the ATP binding rate for the bound trailing head, where ATP binding causes complete detachment from the filament. The observed average duration of 0.49 s again suggests two equal populations, one similar to the previous steps (0.7 s dwell time), and one with a dwell time of 0.35 s, corresponding to the expected binding rate of ATP at 3 μM ATP.

Consistent with this description, we calculate average run lengths of 7.6 and 6.9 double steps (74 nm) for M5elc and M5cam. These run lengths are about one-third the run lengths

reported by Baker *et al*., for the possible reasons discussed below. We can also calculate an expected run length at saturating ATP of about 8 double steps based on the rates of ADP release (12 s^{-1}) and free head rebinding (180 s^{-1} for M5elc). This value is comparable to the run length of 10 double steps similarly calculated by Rosenfeld *et al.* The run lengths we measure at 3 μM ATP are shorter than expected if the run length was dictated by competition between free head rebinding and ATP binding to the bound head (~3 s^{-1} at 3 μM ATP). We hypothesize that run termination occurs when the free head is prevented from rebinding to the actin filament. Myosin V spirals around the actin filament with a periodicity of 2.2 μm (ref. 3). In 15 steps (7.5 displacements of 74 nm each), the labeled myosin would on average be expected to have rotated 90º, from the top of the filament to the side. Runs may therefore terminate when the gold-labeled myosin V steps around to the side of the filament and runs into the glass surface.

Decay kinetics of the intermediate

The data in figures 2e, S8a, and S9a are shown fit to biexponential curves. As discussed below, the fast rate likely reflects the true rate of free head rebinding, while the slower rate is an empirical fit to rebinding events that are slowed by local steric hindrance. For details on fitting, see Methods.

The complex kinetics of the substep do not stem from separate substep populations with differing dwell times and substep sizes. If this *were* the case, one would expect a correlation between substep size and duration. No such correlation was apparent. The correlation coefficient between substep size and duration was 0.050 for M5elc (194 non-last steps) and 0.10 for M5cam (87 non-last steps). The lack of correlation between substep size and dwell time also argues against, but does not preclude, the interesting possibility that the intermediates of long duration result from species where the front head cannot attach stably to actin, and instead reversibly binds and detaches. If these transient rebinding events were of sufficiently short duration, they might escape detection, both in the inspection of individual events and in the correlation calculated above.

The heterogeneous kinetics observed do not stem from a mixture of molecules with fast and slow intermediates. We computed the binomial probability of observing *m* or more intermediate dwells with lengths above an arbitrary percentage cutoff out of *n* total for a given molecule. A variety of cutoffs were investigated, with the 80th length percentile showing the best

discriminatory power. For M5elc at most 3 molecules, totalling 8 steps, could be found which might leniently be supposed to possess an unusually ($p < 0.1$) large number of slow steps. The inclusion or removal of these data points did not materially alter the total distribution, so they were left in.

Finally, we note that the fast decay is well fit, while the slower points show obvious residuals (Figures 2e, S8a, S9a). This observation suggests that the slower rebinding events result from a variety of processes, not from a well-defined mechanistic pathway.

A more likely explanation is that the rebinding rate is influenced by local heterogeneity, in particular by the influence of the nearby glass surface. As described above, myosin V spirals around the actin filament. The steric hindrance that results when labeled myosin V is near the glass surface might well account for the observed heterogeneity in rates. Uemura *et al.* report that the method of actin attachment to the surface critically affects processive stepping, again indicating that the local environment exerts strong effects on processivity[4].

The effects of BDM and free phosphate on free head rebinding kinetics

Uemura *et al.* also observe the prolongation of a myosin V substep in the presence of BDM, which they attribute to the delay of the power stroke. Previously reported data show that BDM does not hinder ATP hydrolysis or phosphate release.[4] In our data, such a delay would be expected to break the 49 nm substep into displacements of 20 and ~30 nm. Instead, we see only a single, response-limited 49 nm substep (Figure S8b). It seems plausible that, at least under zero load, the prolongation of the intermediate instead results from inhibition of the initial binding step.

The addition of 50 mM free Pi does not alter the free head rebinding kinetics (Figure S9a). This observation suggests either that Pi release is quasi-irreversible, that Pi release does not markedly alter the affinity of myosin V for actin, or that the front head dwells in an ADP Pi state, as has been previously suggested by Baker *et al*. We do not observe a separate power stroke within the 49 nm substep, indicating that Pi release has already occurred at that time. In addition, direct measurements suggest that Pi release is rapid[5], and that the ADPPi-bound myosin V catalytic domain binds relatively weakly to actin[6]. The simplest explanation for our observations is that Pi release is rapid and quasi-irreversible.

Straight vs. bent leg myosin V models

The differences between our results and those of Syed *et al.* and Tropak *et al.* should be viewed with caution. A subtle artefact resulting from the method of gold particle attachment could conceivably obscure the 10 nm steps expected from the straight lever arm model. Importantly, the previous studies used myosin V purified from chick brain, which possesses a different complement of light chains[7] than either M5elc or M5cam. Light chain composition could therefore affect the apparent stepping pattern, especially given that we and others[8] observe light-chain dependent changes in other mechanistic parameters. As in the previous studies, we also find that a lever arm stroke occurs simultaneously with every step[9], as evidenced by the alternating 53 and 21 nm steps we observe in addition to the more common 74/0 nm stepping pattern.

The original report of EM images showing myosin V bound to actin describes ~70% of the dimers has having bent front lever arms[10]. Subsequent reanalysis of the same dataset by Burgess *et al.* yielded 6 classes comprised of 150 front lever arms that are more or less straight[11]. The authors state that the image classification protocol used may have rejected molecules with bent front lever arms due to their heterogeneity. It is not clear what fraction of the total lead head images were rejected from classification, although data for 262 such images are reported by Walker *et al.*

METHODS

Actin and myosin preparation. Actin was prepared as previously described, with the exception that dithiothreitol (DTT) replaced beta-mercaptoethanol[12]. A 10 μM actin stock solution was prepared in assay buffer (AB; 25 mM imidazole, 25 mM KCl, 4 mM $MgCl_2$, 1 mM EGTA) plus 1 mM DTT, 1 mM ATP, 3.3 μM TMR-phalloidin (Invitrogen) and 6.7 μM phalloidin, final pH 7.4.

The chicken myosin Myosin V/GCN4 fusion plus calmodulin was expressed and purified as previously described[13]. The human essential light chain (elc) LC1sa was cloned into the pFastBac vector and converted into a separate virus. Co-infection with the myosin V/calmodulin virus and the LC1sa virus led to the expression of myosin V bearing both calmodulin and elc.

Biotinylated calmodulin. A single cysteine was incorporated into sea urchin vertebrate-like calmodulin via the mutation Q143C, and the protein was expressed and purified as previously described.[13] Q143C calmodulin was transferred into buffer containing 20 mM imidazole, 5 mM $CaCl_2$, pH 7.5 using a BioRad Micro Bio-Spin 6 buffer exchange column, and diluted to a final protein concentration of 6.7 mg mL^{-1}. Biotin-maleimide (Sigma) was prepared as a 50 mM stock solution in dimethylsulfoxide, and added to a final concentration of 0.5 mM. The reaction was then incubated at room temperature for 1 hr, then dialyzed against 10 mM imidazole, 0.5 mM EGTA, 0.5 mM DTT. pH 7.5 overnight at 4 ºC. Biotinylation was confirmed by MALDI-mass spectroscopy. Aliquots were flash frozen and stored at -80 ºC.

Myosin-gold particle conjugation. 40 nm diameter gold nanoparticle-streptavidin conjugates were purchased from Ted Pella, Inc. The particles were washed 3x prior to use by dilution from 30 μL to 1 mL in 2 mM Tris, pH 8.0, followed by centrifugation at 14,000xG for 2 minutes, and resuspension in 30 μL 2 mM Tris, pH 8.0. Unfunctionalized 60 nm particles were first concentrated 10x by centrifugation at 8000xG for 2 minutes, followed by resuspension in 2 mM Tris, pH 8.0. Neutravidin (Invitrogen) was added to a concentration of 2 mg mL^{-1} from a stock of 10 mg mL^{-1}, and the mixture incubated overnight at 4 $^{\circ}$C after the addition of 50 mM Tris pH 8.0. Excess neutravidin was removed using the washing procedure described above.

Myosin V labeled with either 40 or 60 nm gold particles takes processive 74/0 nm steps along actin. Simple theoretical considerations suggest that the time resolution of the experiment might be noticeably better with the smaller particles (see below). Thus, the 60 nm particles were used only to determine step size and dwell time distributions (Figure S3). All the other measurements reported use 40 nm particles.

Biotinylated calmodulin was attached to myosin V following established protocols which yield at most one labeled calmodulin per myosin V dimer.[13] 0.75 μM each wild-type and biotinylated calmodulin were added to exchange buffer: 25 mM KCl, 25 mM imidazole, 4 mM $MgCl_2$, pH 7.5. Myosin V (~70 nM heavy chain) was then added, and the mixture incubated at 22 ºC for 2 minutes. Addition of 1 mM $CaCl_2$ initiated the calmodulin exchange, which was quenched by the addition of 8 mM EGTA after 5 minutes.

Gold particles prepared as above were diluted 2x in ABcam (AB + 5 μM calmodulin). Serial dilutions of the biotinylated myosin V were then added to the Au/ABcam solutions. In practice, a final myosin dimer concentration of ~50 pM yielded good results, with a large fraction of particles exhibiting behavior indicative of single myosin attachment. The final gold particle concentration was ~300 pM, consistent with one or zero myosin dimers per gold particle. Due to day-to-day variability, a range of myosin to gold particle ratios was always tested, and the lowest ratio which still produced moving particles was used. The myosin V-Au conjugates are stable for several hours at 4 $^{\circ}$C.

Flow cell assembly. Glass microscope slides (Gold Seal, cat. no. 3050) were treated in a plasma cleaner (Harrick Plasma) for 1 minute on "high" and a pressure of ~2 Torr. A single flow cell was then assembled using double-sided transparent tape (Scotch) and a No. 1 weight cover slip. A 1 mg mL^{-1} solution of biotinylated PEG-polylysine branch copolymer (SurfaceSolutions Ltd.) in phosphate buffered saline was added to the flow cell, and incubated for 30 minutes. The polymer passivates the surface, but provides weak interactions which immobilize actin. The biotinylation of the PEG-polylysine is unlikely to be important for this assay. After incubation, the flow cell was washed 2x with 15 μL AB, and then 4x with 10 μL 1/20 actin stock diluted in AB. Care must be taken to use gentle, gravity-driven flow to avoid dislodging the filaments.

Excess actin was removed by a 2x wash with 15 μL AB. Au-M5 conjugate was then added (typically 10 μL 1/3 dilution in ABcam) and incubated for 10 minutes to allow rigor binding to the actin filament. Unbound particles were removed with a 15 μL wash with ABcam. 10 μL GO buffer was then added: ABcam plus 3 μM ATP, 100 nM biotin, 0.2 mg mL^{-1} glucose oxidase, 0.4% w/v glucose, 0.04 mg mL^{-1} catalase, 1 mM phosphocreatine, 0.1 mg mL^{-1} creatine phosphokinase, final pH 7.4. Subsaturating ATP was used in all experiments so that transitions associated with ADP release[2] might be observed.

Experiments performed in the presence of 50 mM sodium phosphate, pH 7.5, required an altered flow cell assembly, since the addition of the NaPi caused the actin filaments to release from the slide surface. Accordingly, the slides were plasma cleaned, and then spin-coated (4000 rpm, 40 s) with 0.1% nitrocellulose in *n*-amyl acetate. The coverslip was attached as above, and then 10 uL of a 1/20 dilution of the actin stock solution applied. After 2 minutes, the actin was

washed out, and the cell was incubated in the PEG-polylysine copolymer solution for 30 minutes. The cell was then incubated with 15 uL 10 mg mL^{-1} bovine serum albumin (BSA; Sigma, 99 %) for 2 minutes to further reduce particle sticking. The Au-M5 binding step was performed in the presence of 1 mg mL^{-1} BSA, and the rest of the procedure followed as above.

Microscopy. The flow cell was imaged using darkfield illumination (Figure 1). Illumination was provided by a Coherent DPSS 532 nm 100 mW laser. A 1 OD neutral density filter reduced illumination intensity to ~10 mW. The laser was focused and steered through the flow cell using an 1.2-1.33 NA reflecting ball condenser from Olympus, and scattered light was collected with a 40x 0.9 NA Zeiss water-immersion, fixed-length objective. The image was collected with an Andor DV860 back-illuminated EMCCD camera, at frame rates up to 3125 Hz. The pixel size was calibrated from a 10 μm grid (Technical Instrument Co., San Francisco). The uncertainty in pixel size derived from this calibration is 0.35%, measured as the uncertainty of the mean distance between grid marks. The sample was kept at ambient temperature during data collection: 20 ± 2 ºC.

Data Analysis. Raw data was imported into Matlab, and the spot center for each frame determined using a double Gaussian fit, as previously described[14]. An actin filament, modelled as a second order polynomial, was then fit to the path of the particle. The data shown in Figure 1b, and analyzed throughout the paper, corresponds to the distance traversed along the filament.

In order to characterize the intrinsic noise in the measurement, as opposed to variance resulting from the motion of the Au particle about the Au-M5 connection, we analyzed data collected for 40 immobile particles that were observed during the course of recording most of the data presented in this paper. All analyzed stuck particles were 40 nm Au, recorded at 3125 Hz. 144 ms windows for each particle were selected for localization. On average, the spot centers had *x* and *y* standard deviations of σ_x = 11.6 and σ_y = 10.6 nm over the 144 ms window. The 10% of stuck particles with lowest noise had σ_x = 6.8 nm and σ_y = 5.8 nm. These figures likely represent the current noise limits of the instrument. Using estimates of 6 (generous) to 11 nm (conservative) for the measurement noise generates estimations for the particle motion standard deviations of 10 to 5 nm. If the particle was completely free to rotate and the instrument had infinite bandwidth, the position standard deviation would be 20 nm. Instead, it appears that the

stiffness of the particle-myosin attachment constrains the bead diffusion when both heads are bound to actin.

The relaxation time of a bead rotating about its edge is given by:

$$\tau = \frac{\gamma}{\kappa} = \frac{14\pi r^3 \eta \langle \theta^2 \rangle}{k_B T}$$

Where $<\theta^2>$ is the mean squared angular deviation due to thermal energy as the bead rotates about its edge. A reasonable value for $<\theta^2>$ of $\pi^2/4$ rad^2 yields a relaxation time of ~0.2 ms, comparable to our time resolution. In agreement with this rough calculation, autocorrelation and power spectrum analysis both indicate a roll-off time of 1-2 ms for the 40 nm beads. The slower particle motion as compared to theory may result from the drag effects of the nearby surface or a somewhat increased radius due to the protein coating.

Of the particles that moved along actin, approximately 40% showed regular steps with an average length of 74 nm (Figures 1b, S3). About 5% showed alternating 21 and 53 nm steps (Figure S2), a negligible number showed alternating 40 and 30 nm steps. The remaining particles moved processively, but with irregular, unclassifiable steps. The alternating 74/0 nm stepping pattern is a well-established hallmark of single myosin V processive motion based on numerous single molecule fluorescence experiments[13,15,16,17,18,19,20]. Therefore, these traces were selected for further investigation. The rate of 74 nm steps that we observe matches that predicted from the previously measured ATP binding rate, again indicating that these traces represent single myosin V dimers[21]. The runs with irregular steps may result from a mixture of irregular bead-myosin attachments, multiple beads per motor, multiple motors per bead, or other causes.

The dwell time distribution for 74 nm steps was fit to the expected kinetics in a least-squares sense:

$$R = Ck^2 te^{-kt}$$

where R is the number of 74 nm steps per unit time, k is the underlying rate of ATP turnover, and C is a proportionality constant related to the total number of events recorded. The dwell time distribution was first divided into evenly spaced bins. Bins with less than 5 events

were recursively combined with neighboring bins. The error on k was determined using the bootstrap method[22], and is reported as the standard deviation from the resulting ensemble of values for k (5000 replicons). In addition, we note that the maximum likelihood estimator for k is: $k_{ml} = 2/d_{ave}$, where d_{ave} is the average dwell time between steps.

The 49 nm substep within 74 nm steps was identified by the displacement and the increase in variance. Putative substeps were first identified in the 1D projections along the actin filament, and then corrected based on the segment of the 2D plot corresponding to the step. Position variance within the substep was quantified in two ways. The standard deviation before, during, and after the substep was calculated for each event, and then displayed as a histogram (Figure S5). In addition, data points recorded immediately before, or during, the substep were combined for all the steps, binned into x-y cells, and then graphed as contour plots (Figure 2b). Two variations on this analysis are shown. In Figure 2b, the data recorded during the intermediate are recentered at (0, 0) to remove any contribution of static variability to the observed distributions. In Figure S7b, events were aligned with the starting position at (0, 0), determined as the average of the data points recorded for the 32 ms prior to the step. The distribution of intermediate data points was then calculated without recentering. This yields a measurement of the axial and lateral displacement during the intermediate, as well as an indirect measurement of the static variability of the intermediate in the x and y directions.

The substep dwell times are presented as cumulative lifetime plots, that is, the fraction of substep dwells longer than a given time t. The resulting decay curves fit reasonably well to a biexponential, purely on an empirical basis. We were chiefly interested in the initial, fast rate of decay. Accordingly, we fit the data in a least-squares manner to a monoexponential decay $ae^{-kt} + b$ up to an arbitrary cutoff time. The cutoff time was systematically increased until the effect of slower processes became apparent; k decreased, and obvious residuals appeared in the fit. These cutoff times were 10 ms for M5elc and 50 ms for M5cam, corresponding to 54 and 85 percent of the respective populations. The bootstrap method (5000 replicons) was used to derive error estimates for k, which are reported as the standard deviation of the resulting ensemble of values for k. The distribution of k values derived from the bootstrap analysis is roughly Gaussian in all cases.

Many of the processive runs are interrupted either at the beginning or end by the boundaries of files, or by the molecule walking out of the field of view. In order to calculate an estimate of the average run length, we assumed that the underlying distribution was exponential. We then counted the total number of steps s and of detachments d observed for both M5elc and M5cam. The probability P_d of a run terminating during a given transition is $P_d = d/(s+d)$. The average run length is then $1/P_d$. The run lengths so derived are 7.6 for M5elc (246 74-nm steps, 38 detachments) and 6.9 for M5cam (112 74-nm steps, 19 detachments). Run length distributions include only the data from 74/0 nm steppers, since not enough data was collected for the 53/21 and 40/30 stepping patterns to provide reliable estimates.

REFERENCES

1. Vilfan, A. Elastic lever-arm model for myosin V. *Biophysical J.* **88**, 3792-3805 (2005).
2. Veigel, C., Schmitz, S., Wang, F. & Sellers, J. R. Load-dependent kinetics of myosin-V can explain its high processivity. *Nat. Cell Biol.* **7**, 861-869 (2005).
3. Ali, M. Y. *et al.* Myosin V is a left-handed spiral motor on the right-handed actin helix. *Nat. Struct. Biol.* **9**, 464-467 (2002).
4. Uemura, S., Higuchi, H., Olivares, A. O., De La Cruz, E. M. & Ishiwata, S. Mechanochemical coupling of two substeps in a single myosin V motor. *Nat. Struct. Mol. Biol.* **11**, 877-883 (2004).
5. Rosenfeld, S. S. & Sweeney, H. L. A model of myosin V processivity. *J. Biol. Chem.* **279**, 40100-40111 (2004).
6. Yengo, C. M., De La Cruz, E. M., Safer, D., Ostap, E. M. & Sweeney, H. L. Kinetic characterization of the weak binding states of myosin V. *Biochemistry* **41**, 8508-8517 (2002).
7. Espindola, F. S. *et al.* The light chain composition of chicken brain myosin-Va: calmodulin, myosin-II essential light chains, and 8-kDa dynein light chain/PIN. *Cell Motil. Cytoskeleton* **47**, 269-281 (2000).
8. De La Cruz, E. M., Wells, A. L., Sweeney, H. L. & Ostap, E. M. Actin and light chain isoform dependence of myosin V kinetics. *Biochemistry* **39**, 14196-14202 (2000).
9. Forkey, J. N., Quinlan, M. E., Shaw, M. A., Corrie, J. E. & Goldman, Y. E. Three-dimensional structural dynamics of myosin V by single-molecule fluorescence polarization. *Nature* **422**, 399-404 (2003).
10. Walker, M. L. *et al.* Two-headed binding of a processive myosin to F-actin. *Nature* **405**, 804-807 (2000).
11. Burgess, S. et al. The prepower stroke conformation of myosin V. J. Cell Biol. 159, 983-991 (2002).

12. Pardee, J. D. & Spudich, J. A. Purification of muscle actin. *Methods Enzymol.* **85 Pt. B**, 164-181 (1982).
13. Churchman, L. S., Ökten, Z., Rock, R. S., Dawson, J. F. & Spudich, J. A. Single molecule high-resolution colocalization of Cy3 and Cy5 attached to macromolecules measures intramolecular distances through time. *Proc. Natl. Acad. Sci. USA* **102**, 1419-1423 (2005).
14. Ökten, Z., Churchman, L. S., Rock, R. S. & Spudich, J. A. Myosin VI walks hand-over-hand along actin. *Nat. Struct. Mol. Biol.* **11**, 884-887 (2004).
15. Yildiz, A. *et al.* Myosin V walks hand-over-hand: single fluorophore imaging with 1.5-nm localization. *Science* **300**, 2061-2065 (2003).
16. Warshaw, D. M. *et al.* Differential labeling of myosin V heads with quantum dots allows direct visualization of hand-over-hand processivity. *Biophys J.* **88**, 30-32 (2005).
17. Syed, S., Snyder, G. E., Franzini-Armstrong, C., Selvin, P. R. & Goldman, Y. E. Adaptability of myosin V studied by simultaneous detection of position and orientation. *EMBO J.* **25**, 1795-1803 (2006).
18. Toprak, E. *et al.* Defocused orientation and position imaging (DOPI) of myosin V. *Proc. Natl. Acad. Sci. USA* **103**, 6495-6499 (2006).
19. Snyder, G. E., Sakamoto, T., Hammer, J. A., Sellers, J. R. & Selvin, P. R. Nanometer Localization of Single Green Fluorescent Proteins: Evidence that Myosin V Walks Hand-Over-Hand via Telemark Configuration. *Biophysical J.* **87**, 1776-1783 (2004).
20. Sakamoto, T., Yildiz, A., Selvin, P. R., Sellers, J. R. Step-Size Is Determined by Neck Length in Myosin V. *Biochemistry*, **44**, 16203-16210 (2005).
21. De La Cruz, E. M., Wells, A. L., Rosenfeld, S. S., Ostap, E. M. & Sweeney, H. L. The kinetic mechanism of myosin V. *Proc. Natl. Acad. Sci. USA* **96**, 13726-13731 (1999).
22. Efron, B. & Tibshirani, R. J. *An Introduction to the Bootstrap* (Chapman & Hall/CRC, New York, 2000).